AIAA-2010-2578

2010 AIAA SDM Student Symposium
51st AIAA/ASME/ASCE/AHS/ASC Structures, Structural Dynamics, and Materials Conference
12–15 April 2010, Orlando, Florida

New Structural Design Concepts for Large Thermoplastic Wind Turbine Blades Using Structural Optimization Techniques

Louis-Charles Forcier* and Simon Joncas†

École de technologie supérieure, Montréal, Québec, H3C 1K3, Canada

This paper presents a structural optimization process for the design of large thermoplastic wind turbine blades. Previous work by one of the authors on topology optimization of a short section of a blade has shown that a structure with a box spar and ribs is optimal to minimize the compliance for a given amount of material. The optimization process presented in this paper consists of topology optimization on the inner half of a blade with the inner volume of the blade as the design domain. Result of this problem (number and position of shear webs and ribs) are then interpreted to build a shell model of the complete blade to perform composite size optimization based on a minimum mass objective subjected to constraints on deflection, composite strength and structural stability. Different blade models using ribs are then optimized and compared against conventional blade structure (spar box without ribs, single web without ribs). The use of ribs in wind turbine blade structures, which is more adapted to thermoplastic composite manufacturing, leads to slightly lighter blades than conventional blade structures.

Nomenclature

Acronyms

BEM	Blade element momentum
EDC_{50}	50 years recurrence extreme direction change
EWM	Extreme wind speed model
EWS	Extreme wind shear
IEC	International Electrotechnical Commission
NWP	Normal wind profile model
PA-6	Polyamide-6
SIMP	Solid Isotropic Material with Penalization
TPC	Thermoplastic compostite
UD	Unidirectional

Latin variables

c	Chord length, m
c_j	Compliance of the structure for load case j, Nm
c_{max}	Maximum chord length, m
dF	Load per unit length of the blade, N/m
E	Modulus of elasticity, GPa
E_1	Longitudinal modulus of elasticity, GPa
E_2	Transverse modulus of elasticity, GPa
$\mathbf{f}$	Nodal load vector of a finite element problem, N
F_{je}	Composite failure index of element e under load case j
G_{12}	Shear modulus, GPa
h	Wind turbine hub height, m
$\mathbf{K}_e$	Baseline stiffness matrix of a finite element, N/m
$\tilde{\mathbf{K}}_e$	Modified stiffness matrix of a finite element, N/m
m	Mass, kg
M	Bending moment, Nm
M_{max}	Maximum bending moment, Nm
n	Number of design variable in the optimization problem
n_e	Number of elements in a finite element problem
n_j	Number of load cases

*Graduate student, École de technologie supérieure, Department of Mechanical Engineering, 1100 Notre-Dame W., Montréal, Québec, H3C 1K3, Canada.

†Assistant professor, École de technologie supérieure, Department of Automated Manufacturing Engineering, 1100 Notre-Dame W., Montréal, Québec, H3C 1K3, Canada.

Link to the final published version: https://doi.org/10.2514/6.2010-2578

n_k	Number of buckling mode extracted
p	Penalty factor for the SIMP approach topology optimization
P	Power, W
r	Radial position on the wind turbine blade, m
R	Radius of the wind turbine rotor, m
S_1^C	Compressive longitudinal strength, MPa
S_2^C	Compressive transverse strength, MPa
S_1^T	Tensile longitudinal strength, MPa
S_2^T	Tensile transverse strength, MPa
S_{12}	In-plane shear strength, MPa
t	Thickness, mm
$\mathbf{u}$	Displacement vector of a finite element problem, N
V	Shear force, N
V_{out}	Cut-out wind speed, m/s
V_r	Rated wind speed, m/s
$V(\rho_e)$	Volume of material in a topology optimization problem, m^3
V_0	Volume of the design domain in a topology optimization problem, m^3
$\mathbf{x}$	Design variable vector

Greek variables

δ_j	Deflection of blade tip under load case j, m
$\theta_{p,0}$	Blade pitch angle, deg.
θ_T	Blade twist angle, deg.
λ	Blade tip speed ratio
λ_{jk}	Buckling factor for the k^{th} mode under load case j
ρ	Material density, kg/m^3
ρ_e	Element density for a topology optimization problem
Ψ	Azimuth angle, deg.
Ω	Rotor speed, rad/s or rpm

I. Introduction

In retrospect, the last 30 years of thermosetting composite wind turbine blade development yielded three distinct structural concepts: the monolithic skin monocoque concept (based on Ulrich Hutter's pioneering design (1959)), the single shear web design, and the double shear web or box spar concept (see figure 1). The last three decades also saw non-negligible improvements in manufacturing techniques while most manufacturers moved from the classic hand lay-up process to vacuum infusion methods or pre-pregging.[1] From a material point of view, measures were also taken to improve the design. New glass fabrics were introduced and meticulous use of carbon fibers for highly stressed areas is now common in large blades. Resin systems also evolved from basic polyester-based systems to vinylester and epoxy systems.[2] Finally, numerous improvements were also made to blade root details with manufacturers refining their design from first generation heavy one-piece metallic flanges to lighter flange designs and bonded-in sleeves and stud connections. As a result of these improvements, thermosetting composite blade weight with respect to length was remarkably well controlled by designers and manufacturers. Theoretically, if materials and structural concept are kept unchanged during an up-scaling process, mass should evolve as a cubic function of blade length. On the contrary, due to the above mentioned improvement to the design, manufacturing processes and materials, blade mass scaled closer to a square law over the years.[1]

Due to the impressive growth rate of the wind energy industry, the wind energy composite market has witnessed an impressive steady growth rate of 20 % the last couple of years and is now consuming close to 250 000 tons of composite materials per year.[3] As a consequence of blade design life being limited to 20 years, blade scrap should be in the same order of magnitude in weight by 2025 and rising every year by 20 %. Judging from these numbers, it is obvious that the industry will have to take their responsibilities regarding recycling. Unfortunately, since thermosetting resin are not well suited for primary recycling, it is possible that the industry will be forced to switch to more sustainable resin systems as it was the case for the European automotive composite industry when the vehicle end-of-life legislation came into effect.

In this context, this paper presents a design solution for large, fully recyclable, thermoplastic composite blades. Since thermoplastic composites (TPC) are processed differently than their thermosetting counterpart, the design solution was not based on existing blade designs but rather developed using structural optimization techniques. Previous work on topology optimization of a wind turbine blade section has shown that the introduction of ribs in the blade structure could be a good concept to maximize stiffness.[4] Based on these results and the fact that TPC ribs, multiple skin panels or stringers could be produced with fast non-isothermal melt processes, this paper explores different TPC blade designs using a 2 steps optimization strategy.

The following sections will present blade geometry, the load cases studied and the optimization strategies used to generate these thermoplastic composite oriented design solutions. Finally, the different designs will be compared and a final design will be proposed.

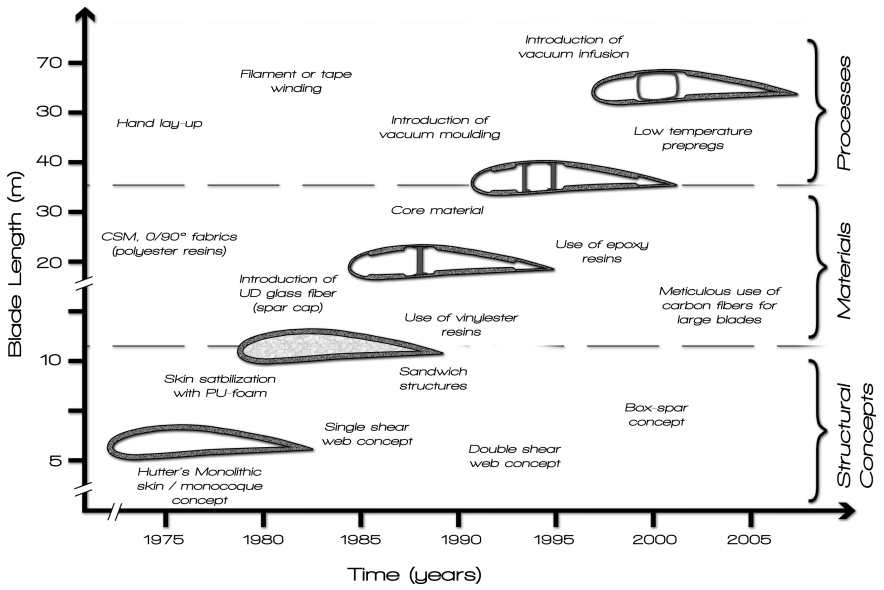

Figure 1. Structural design concepts, materials and processes evolution of thermosetting fiber-reinforced composite wind turbine blades (1975-now).

II. Blade geometry

Targeting next generation wind turbines, the blade studied in this paper is meant for a 150 m, 3-bladed, up-wind, variable speed and pitch regulated wind turbine. The nominal power (P) of the turbine is 8 MW at a rated wind speed (V_r) of 12 m/s. The blade tip speed ratio (λ) is 7.5 up to rated wind speed. Between this wind speed and the cut-out wind speed (V_{out}) of 25 m/s, the rotational speed is fixed at Ω=11.5 rpm. For this study, the hub height (h) is set at 150 m.

The blade's aerodynamic shape chosen for this study was adapted from van Rijswijk et al.[5] and Joncas et al.[6] and is based on current large wind turbine blade geometric trends. The maximum chord length (c_{max}) is set to 7.5 % of blade length and is situated at 20 % of the rotor radius (R). The chord at tip is 20 % of the maximum chord length and the distribution of chord is linear from the maximum chord position to blade tip. The hub radius is 5 % of the rotor radius and the blade root diameter is set as 70 % of c_{max}. The distribution of twist is non-linear and is set to yield the design angle of attack in each blade elements.

Airfoils used for the aerodynamic part of the blade (from maximum chord position to tip) are DU series developed at Delft University of Technology for wind turbines.[7] Four different airfoils are used to allow a higher thickness to chord ratio in the highly loaded region near the root and a lower thickness to chord ratio near the tip. The region between the root and the maximum chord position evolves from a circular section to an airfoil shape. Table 1 shows the blade geometry where r is the radial position of the chord station relative to the rotor's axis of rotation, c is the chord length and θ_T is the twist angle. The blade pitch angle $\theta_{p,0}$ (defined as the angle between the rotor plane and the blade tip chord line) is -2° for wind speeds under 12 m/s (rated wind speed) and is adjusted to regulate power to 8 MW for wind speeds above V_r.

III. Design Loads

Loads on the wind turbine blade have been determined according to the IA wind class of the International Electrotechnical Commission 61400-1 standard.[8] This standard defines 8 different design situations for which the integrity of the turbine has to be validated: power production; power production plus occurrence of fault; start up; normal shut down; emergency shut down; parked (stand still or idling); parked and fault condition; transport, assembly, maintenance and repair. Obviously, since this paper deals with preliminary

Table 1. Blade geometry with corresponding airfoils.

r [m]	c [m]	θ_T [°]	Airfoil
3.750	3.938	-	Circle
15.000	5.625	21.2	DU-97-W-300
21.667	5.125	13.1	DU-97-W-300
28.333	4.625	8.2	DU-97-W-300
35.000	4.125	4.3	DU-91-W2-250
41.667	3.625	3.3	DU-00-W-212
48.333	3.125	2.1	DU-00-W-212
55.000	2.625	1.3	DU-96-W-180
61.667	2.125	0.7	DU-96-W-180
68.333	1.625	0.1	DU-96-W-180
75.000	1.125	0.0	DU-96-W-180

blade design, a large number of these design situations are impossible to evaluate since they require full wind turbine characteristics to be known (control systems, tower/foundation design, etc.). Therefore, this study will only consider specific power production situations and parked design situations where only blade characteristics are sufficient to evaluate the design situation. The following two sections will present these design situations and corresponding load cases.

III.A. Power production design situation

For the power production design situation, the IEC 61400-1 standard defines 9 load cases ranging from normal wind profile driven load cases to extreme wind shear driven load cases. Again, a large number of these load cases require wind turbine design characteristics not available when at the stage of preliminary blade design (yaw alignment system speed, pitch control system speed, ...). Therefore, out of the 9 load cases described, only the load cases using the following three wind conditions were evaluated :

- Normal wind profile model (NWM)
- Extreme wind shear :
  - horizontal negative extreme wind shear (EWS(HN))
  - horizontal positive extreme wind shear (EWS(HP))
  - vertical extreme wind shear (EWS(V))
- 50 years recurrence extreme direction change:
  - negative extreme direction change (EDC_{50}(N))
  - positive extreme direction change (EDC_{50}(P))

All load cases mentioned above have been evaluated at rated and cut-out wind speeds using AeroDyn[9] and YawDyn.[10] YawDyn analyses the dynamic behavior of the blades of a horizontal axis wind turbine and calls the AeroDyn software to compute the aerodynamic loads on the blades using the blade element momentum theory. YawDyn allows different ways to model the rotor. For this project, we chose to model the out-of-plane bending of the blades by considering them to be infinitely rigid with a torsional spring on their roots ("hinge" hub model in YawDyn) to simulate out-of-plane bending stiffness. The stiffness of the torsional spring was evaluated using the natural frequency of the blade evaluated with tools developed by van Rijswijk et al.[5] To compare the different load cases, we used the maximum bending moment at blade root (M_{max}) given by YawDyn (see table 2). The azimuth angle (Ψ, which is 0 when the blade is pointing downward) of the blade when the maximum bending moment is reached is also presented in table 2. These bending moments take into account aerodynamics, gravitational, inertial and dynamic loads.

The critical load cases are found to be those submitted to an extreme wind shear (EWS). The maximum in-plane load is found with a horizontal negative extreme wind shear, when the blade is at the horizontal

Table 2. Out-of-plane and in-plane bending moments computed using YawDyn for the different power production load cases.

Load cases	out-of-plane		in-plane	
	M_{max} [Nm]	Ψ [°]	M_{max} [Nm]	Ψ [°]
NWP(0), rated	15 204 600	186	7 248 790	266
NWP(0), cut-out	4 417 490	188	6 851 180	260
EWS(V), rated	21 163 500	224	8 289 970	244
EWS(HN), rated	19 230 500	233	9 144 540	270
EWS(HP), rated	19 601 500	142	7 248 930	266
EWS(V), cut-out	13 972 900	190	9 916 490	221
EWS(HN), cut-out	11 936 700	260	11 533 800	264
EWS(HP), cut-out	12 217 700	110	6 851 300	261
EDC_{50}(N), rated	15 288 000	205	7 315 340	267
EDC_{50}(P), rated	15 204 500	186	7 248 790	266
EDC_{50}(N), cut-out	4 417 490	188	6 851 180	260
EDC_{50}(P), cut-out	5 574 100	191	6 917 930	257

position on the side where the aerodynamic forces are in the same direction as the gravity loads and when the wind shear generates the highest wind speed. The vertical extreme wind shear produces the maximum out-of-plane bending moment when the blade is about 45° away from being in the upward position. One of the reasons why the maximum load does not happens when the blade is pointing upward (and submitted to highest wind speed due to wind shear) is that in that position, the wind speed in some blade sections is high enough to cause aerodynamic stall so the loads are reduced. Dynamic effects can also cause a delay between the maximum wind field on blade and the maximum bending moment at blade root.

III.B. Parked design situation

The parked situation loads have been computed with a MATLAB program. Two situations were simulated: one with the blade in the vertical position (pointing upward) and the other in the horizontal position (to add the gravity loads to the aerodynamics load). Both situations where computed with the 50 years extreme wind speed model (EWM). For the vertical blade case, wind coming from all directions was considered since the nacelle and blades are considered fixed. For the horizontal blade case, any pitch angle between -2° (pitch angle for wind speed under rated speed) and 90° (angle corresponding to the fully feathered position) were considered. The fact that a wind turbine fault can occur so that the blade is not in the fully feathering position when the extreme wind occurs is then taken into account.

As for the power production situation load cases, the bending moments (including gravitational loads) at root have been used to compare the loads. Here, to be able to compare loads with the power production situation, a flapwise/edgewise system was used in which the flapwise and edgewise directions correspond respectively to the out-of-plane and in-plane directions when the blade is in the nominal pitch position (0.9° as in section III.A for rated wind speed load cases). The maximum flapwise load (28 889 351 Nm) was found when the blade is at the vertical position and the pitch angle is -2° (blade is perpendicular to the wind direction). The maximum edgewise load (8 092 833 Nm) happens when the blade is in the horizontal position and the pitch angle is 57°.

III.C. Load cases for the optimization problem

For the optimization problem, the four most critical load cases presented in the two last sections were considered :

- Load case 1: Vertical EWS with blade pointing in the upward direction, nominal wind speed (maximum power production out-of-plane root bending moment);
- Load case 2: Horizontal EWS with blade positioning horizontally, cut-out wind speed (maximum power production in-plane root bending moment);

- Load case 3: EWM with the blade pointing upward and perpendicular to the wind (maximum parked flapwise root bending moment);
- Load case 4: EWM with the horizontal blade at a pitch angle of 57° (maximum parked edgewise root bending moment);

Note that for simplicity of modeling, we considered that the maximum load for load case 1 happens when the blade is pointing upward and not at an azimuth angle of 224° as calculated by YawDyn.

Although root bending moment could be considered similar for some load cases, it is important to note that these load cases are very different from each other. In power production load cases, most of the aerodynamic load comes from the outer part of the blade while most of the load come from the inner part of the blade in the parked design situations. Also, load cases with blade pointing upward produce loads that are larger in the flapwise direction than in the edgewise direction while cases with blades positioned horizontally produce loads that are in the same order of magnitude (including gravity) in both directions. Because they are very different in nature, all of these load cases were kept for the optimization process to be sure that the optimized design will be able to support the different loads it is subject to.

Aerodynamic loads along the blade length for the selected load cases (including load cases evaluated with YawDyn) used for the finite element models have been computed using blade element momentum (BEM) theory[11] coded in Matlab. This code does not take into account the dynamic effects of out-of-plane bending so loads of load case 1 have been increased by 10 % in the finite element models because further studies in YawDyn shows that for this particular load case, dynamic effects increase the loads by 10 %.

The applied aerodynamic loads, shear force and bending moment diagrams for each load case are shown in figure 2 to 5. According to the IEC 61400-1 standard, loads presented in this section have been increased by a safety factor when transfered to the finite element model. These safety factors are: 1.35 for the aerodynamic and gravity loads and 1.25 for the inertial loads.

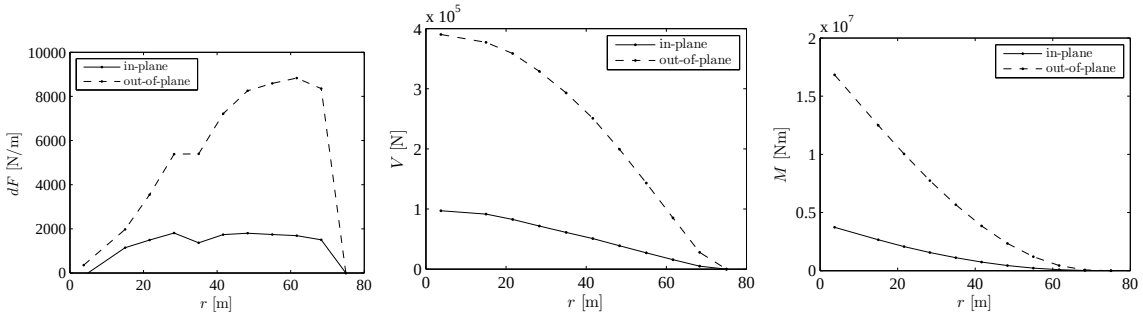

Figure 2. Aerodynamic loads for load case 1 (vertical EWS with blade pointing in the upward direction, nominal wind speed). From left to right: applied load (dF), shear force (V) and bending moment (M).

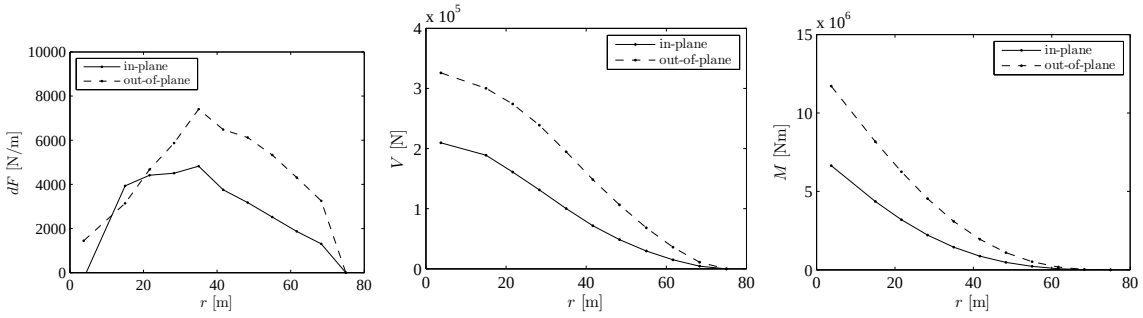

Figure 3. Aerodynamic loads for load case 2 (horizontal EWS with blade positioning horizontally, cut-out wind speed). From left to right: applied load (dF), shear force (V) and bending moment (M).

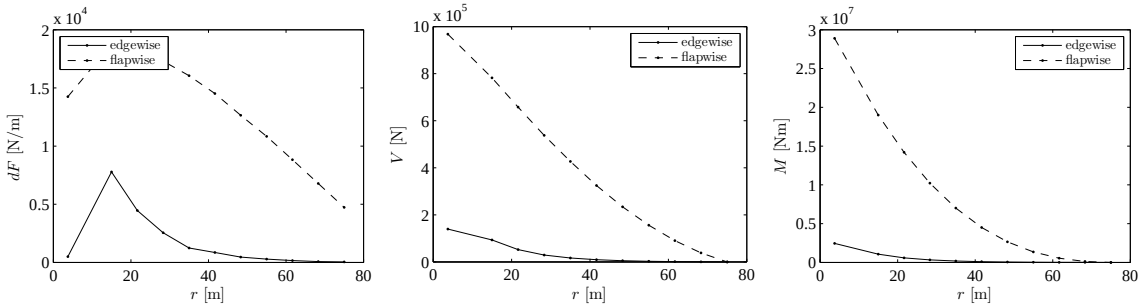

Figure 4. Aerodynamic loads for load case 3 (EWM with the blade pointing upward and perpendicular to the wind). From left to right: applied load (dF), shear force (V) and bending moment (M).

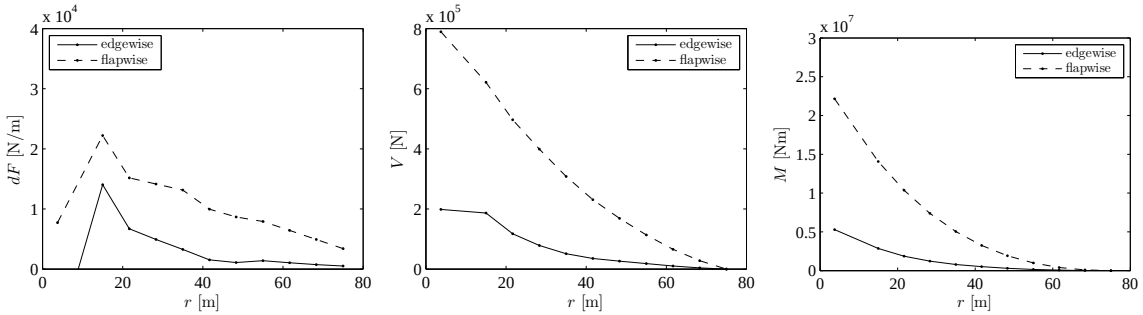

Figure 5. Aerodynamic loads for load case 4 (EWM with the horizontal blade at a pitch angle of 57°). From left to right: applied load (dF), shear force (V) and bending moment (M).

IV. Methodology for the optimization process

The optimization process in this project is separated in two steps. The first step involves topology optimization performed on a design domain consisting of solid tetrahedral finite elements filling the entire inner volume of the blade. The purpose of this step is to roughly show where material should be put to best sustain the applied loads. The objective function of this problem is set to minimize the compliance of the structure (i.e. maximize the stiffness) when constrained to use only a given fraction of the design domain volume (in this case, 20 % is used). The results of this optimization problem gives an idea of the optimal material distribution when using a stiffness criterion. Structural topologies found from this step are then interpreted to be used in the second step of the optimization process.

In this step a new model is used to optimize the thickness of different composite layers when the objective is to minimize the blade mass when constrained on strength, stiffness and stability. The optimization process just discussed is summarized in table 3. This optimization strategy is performed with Altair's Optistruct finite element and optimization solver.

Table 3. Optimization process.

	Step 1	Step 2
Optimization type	Topology	Size
Design variables	Density* of every solid elements	Thickness of composite layers
Constraints	Fixed material volumic fraction	No composite failure, limited deflection and no buckling
Objective	Minimize compliance	Minimize mass

* Here, the density is not the actual material density but a variable in the optimization problem. This concept will be explained in the next section

V. Topology optimization on a solid element model

V.A. Finite element model and optimization problem formulation

The finite element model for topology optimization is shown on figure 6. To lighten the model, only the section from the root to the 35 m radial position (47 % of blade length) was modeled. The upper and lower surfaces of the blade are meshed with 4-node quadrilateral shell elements and the surfaces at both ends are meshed with 3-node triangular shell elements. The closed volume formed by these shell elements is filled with 4-node tetrahedral solid elements. These solid elements form the design domain for the topology optimization problem.

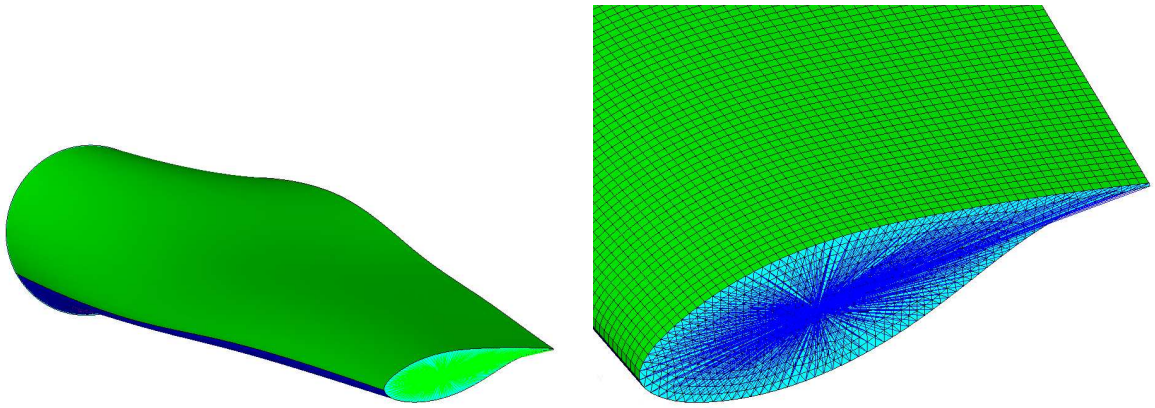

(a) (b)

Figure 6. Finite element model of the blade for topology optimization. (a) Blade without mesh. (b) Zoom at the 35 m radial position (where the blade is cut-off).

The blade is clamped at its root contour and a rigid body element is created on the 35 m radial position to apply the equivalent loads normally applied on the outboard blade sections. All nodes at 35 m chord station are connected to a master node (with all degrees of freedom constrained) on which equivalent shear forces, bending moments and normal forces are applied to simulate the aerodynamic, gravitational and inertial loads of the outboard section of the blade. Aerodynamic loads are applied in the finite element model using a MATLAB program. This program extracts the aerodynamic loads to be applied from the BEM code earlier discussed and then reads the connectivity tables (position of nodes and connectivity of elements) of the finite element model to apply the proper pressure on each shell elements of the upper and lower surfaces of the blade. For a given radial position, the pressure applied is constant over the chord length.

The properties of the shell elements have been given a very low stiffness ($E = 1 \times 10^{-6}$ GPa) and thickness (1 mm). This is done so the shells do not contribute to the structure stiffness and are just used to apply the aerodynamic loads. The design domain (solid elements) uses isotropic material with a Young's modulus of 1000 GPa and a Poisson's ratio of 0.3. This rigidity is much higher than any material used on wind turbine blades but its value does not affect the results of this kind of optimization problem. The reason why this value was chosen is to avoid a too large compliance at the first iteration (when the structure is not optimized) which creates problems when solving. Concerning material density, shell elements have no mass whereas the density of material for solid element is adjusted to get a total mass of the blade of 35 000 kg (in accordance with today's blade mass evolution trend).[5] This enables gravitational and centrifugal force to be modeled directly as volumic loads in the FE model.

The design variables for the optimization problem are the densities of each solid elements. These densities (ρ_e, should not be confused with the material density) vary from 0 to 1 to modify the elements' stiffness as follow :

$$\tilde{\mathbf{K}}_e = \rho_e^p \mathbf{K}_e \tag{1}$$

where $\mathbf{K}_e$ and $\tilde{\mathbf{K}}_e$ are respectively the baseline and modified stiffness matrix of the element and p is a penalty factor that helps avoid intermediate values of ρ_e (forces values to 0 or 1). Thus, when an element density is 0, the stiffness of this element is nil (absence of material). When the density is 1, the baseline material properties are applied to the element. As the optimization process progresses, the density of elements that are not useful to the objective function or to respect the constraints will decrease and the density of useful

elements will increase so that the distribution of densities at the end of the computation shows where material is most needed and where it is not. Unfortunately, even with a penalty factor (with common values varying from 2 to 4) intermediate values of density can subsist. This approach for topology optimization is called "density method" or "Solid Isotropic Material with Penalization" (SIMP). More details on this method can be found in Bendsøe and Sigmund's book[12] and details on the implementation of SIMP method in Altair's OptiStruct solver can be found in articles by Zhou et al.[13] and Thomas et al.[14] and in the OptiStruct documentation.[15]

The objective of the optimization problem is to minimize the sum of the compliance of all load cases (defined in section III.C) with a constraint of 0.2 on the volumic fraction of material contained in the design domain. 20 % of the blade volume is then forced to be kept to maximise the structure's stiffness for all load cases defined in the previous section. The problem can be expressed as :

$$\begin{aligned} \min_{\rho_e} \quad & \sum c_j & & j = 1, ..., n_j \\ \text{subjected to:} \quad & \frac{V(\rho_e)}{V_0} = 20\ \% & & \\ & 0.0 \leq \rho_e \leq 1.0 & & e = 1, ..., n_e \end{aligned} \tag{2}$$

Where c_j is the compliance of load case j, n_j is the number of load cases (4), V_0 is the volume of the design domain, $V(\rho_e)$ is the volume of the design domain occupied by material and n_e is the number of elements in the design domain. The compliance for a load case is computed as the compliance of the full structure (solid design elements and shell elements) and is equal to the strain energy of the structure. In a finite element model, the compliance is computed as :

$$c_j = \frac{1}{2}\mathbf{f}^T\mathbf{u} \tag{3}$$

where $\mathbf{f}$ is the load vector and $\mathbf{u}$ is the nodal displacement vector of the finite element problem.[15] Note that some authors define the compliance as twice the value of the strain energy ($c_j = \mathbf{f}^T\mathbf{u}$).[16]

V.B. Results

The results of this optimization problem are shown in figure 7 as a contour plot of the elements' density at the last iteration. High density regions show places where material is needed and low density regions show places where material is less necessary. As expected, it can clearly be seen on figure 7a that a structure with 2 spar caps emerges to support the load that his predominantly in the out-of-plane direction. These spar caps are situated in the thickest part of each cross section to maximize sectional inertia.

The location of shear webs is a bit harder to interpret. As it can be seen on figure 7b, in some sections, a single web is situated at approximately 1/3 of the chord length (typical for small and medium size blades) while for other sections, there is no web. Nevertheless, a clear closed spar structure (typical for large wind turbine blades) can not be identified.

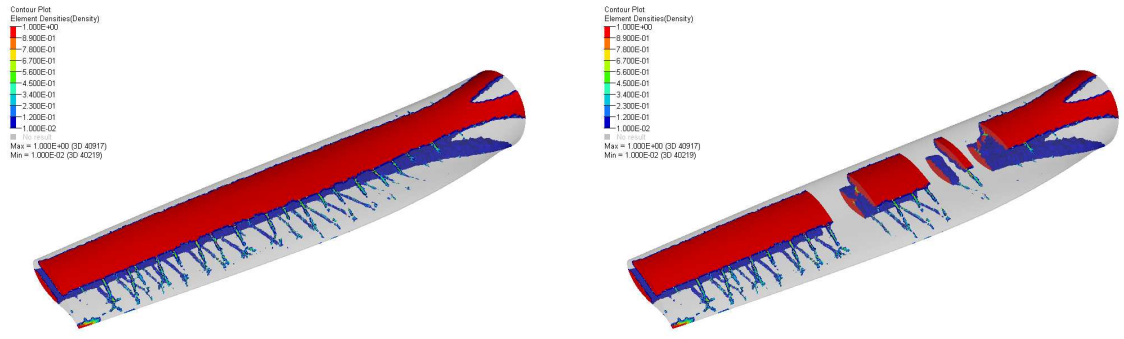

(a) (b)

Figure 7. Result of the topology optimization (density contour plot of design elements), only region with a density higher than 0.1 are shown. (a) Full model. (b) Full model with sectional cuts to show the presence of webs.

We can also see on figures 7a and 7b that at the root of the blade, each spar cap splits in two sections. The blade is then attached to the root by four members symmetrically arranged (see figure 8). This topology

offers a higher edgewise section modulus than if the two spar caps simply continued until they reached the root. This root attachment configuration gives approximately the same section modulus in the edgewise direction than in the flapwise direction.

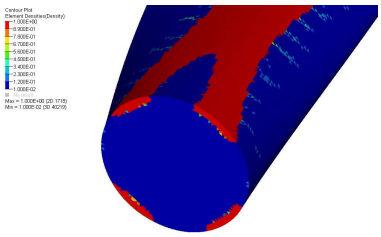

Figure 8. Result of the topology optimization (density contour plot of design elements) in the root region.

An other interesting structural element that can be observed in figure 7 is the presence of ribs in the trailing edge section. These ribs are separated by a distance of 1 to 2 m. The density of these ribs vary from about 0.1 to 0.3. Even if the density of these members is very low, they appear in a region of near zero density which justifies their presence to support the pressure loads applied in the trailing edge region and reduce the distortion of aerodynamic profiles. These results are consistent with previous results obtained on a short untwisted and constant chord blade section using a similar methodology.[4]

In general, the spar cap structure seen on figure 7 is a classic structure for wind turbine blades. However, ribs are not seen in today's large size wind turbine blades but should be well adapted for thermoplastic composite processing. Based on these results, the second step of the optimization process concentrates on refining the design using size optimization on shell elements to study the usefulness of these structural members. The shear web configuration will also be studied.

VI. Sizing optimization on shell model

VI.A. Finite element model and optimization problem formulation

As the number and the location of the shear webs are not clear from the results just shown, it was chosen to build a model with 3 webs situated at 15, 33 and 50 % of the chord length (see figure 9b). It is then possible to remove the central web of the finite element model to analyse a model with two shear webs or to remove the forward and aft webs to analyse a model with only one shear web. Ribs were placed at intervals of 1 m. Again, it is also possible to remove some ribs from the finite element model to compare different possibilities of rib number and spacing.

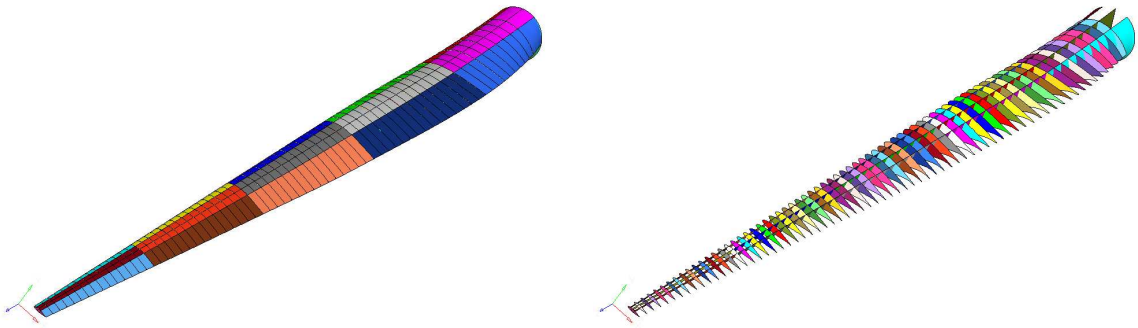

(a) (b)

Figure 9. Shell finite element model of the blade. (a) Exterior shape. (b) interior shape.

The geometry is splited into several areas (115 in total) for which a different composite laminate was defined (different colors in figure 9). The optimization problem is formulated as composite sizing optimization. For every areas, a composite laminate made of 2 layers (a 0° lengthwise unidirectional layer and a ±45° biaxial layer) of polyamide-6 (PA-6, a thermoplastic polymer)/glass fibers and 1 layer of foam core is defined. For ribs (where 0° means chordwise), a 90° unidirectional layer is added to the laminate. The properties

of these materials are presented in table 4. As core material rigidity and strength are not included in the finite element formulation, only density is needed. To compare results with classic blade designs, topologies without ribs have been also modeled with epoxy-based composites for which properties are also presented in table 4. In the finite element model, the strength values have been divided by a safety factor of 1.82, the most severe material safety factor according to the IEC 61400-1 standard.

Table 4. Properties of materials for the sizing optimization.

			PA-6/Glass		Epoxy/Glass		Core[17]
			UD[5]	biaxial[18]	UD[19]	biaxial[18]	
Density	ρ	[kg/m^3]	1770	1800	1880	1820	100
Longitudinal modulus of elasticity	E_1	[GPa]	38.0	26.0	39.2	25.2	
Transverse modulus of elasticity	E_2	[GPa]	8.24	26.0	14.5	25.2	
Shear modulus	G_{12}	[GPa]	1.80	4.10	4.83	3.48	
Tensile longitudinal strength	S_1^T	[MPa]	869	495	830	476	
Tensile transverse strength	S_2^T	[MPa]	32.0	495	53.9	476	
Compressive longitudinal strength	S_1^C	[MPa]	634	473	523	392	
Compressive transverse strength	S_2^C	[MPa]	72.9	473	165	392	
In-plane shear strength	S_{12}	[MPa]	65.5	127	78.1	93.5	

The design variables in this optimization problem are the thicknesses of each layer of each area. These thicknesses can vary from a near zero value (1×10^{-6} m) to a value of 0.100 m. The option used for computation of the composite laminate properties in the OptiStruct finite element code (SMCORE) was set to homogenize the properties of the composite layers (except for the core) which makes the laminate properties independent of the stacking sequence. This way, it is possible to define only two or three composite layers to determine the thickness needed for each. This option is valid only when there is no bending in the composite shells but since the blade is a hollow structure, we suppose that every shell is solicited mostly by in-plane loads. The shell thicknesses obtained with this method can then be easily interpreted as a number of plies if the thickness of each individual ply is known.

To determine shell thicknesses, the objective function is set to minimize the mass of the structure while being subjected to these constraints :

- The Composite failure index must stay below 1.0 in every elements;
- The blade tip deflection must stay below 10 m (13 % of its length);
- The Buckling factor must be at least 1.0 (no buckling allowed).

This optimization problem can be formulated as :

$$\begin{array}{rll} \min\limits_{\mathbf{x}} & m & \\ \text{subjected to:} & \delta_j \leq 10.0 \text{ m} & j = 1, ..., n_j \\ & \lambda_{jk} \geq 1.0 & j = 1, ..., n_j,\ k = 1, ..., n_k \\ & F_{je} \leq 1.0 & j = 1, ..., n_j,\ e = 1, ..., n_e \\ & 0.0 \text{ mm} \leq x_i \leq 100.0 \text{ mm} & i = 1, ..., n \end{array} \tag{4}$$

where m is the blade mass, δ_j is the deflection of the blade tip under load case j, λ_{jk} is the buckling index of the k^{th} mode under load case j and F_{je} is the Tsai-Wu failure criterion of element e under load case j. n_j is the number of load case (4), n_k is the number of modes extracted for each load case (5), n_e is the number of finite elements in the model and n is the number of design variables ($\mathbf{x} = x_1, ..., x_n$). Table 5 shows the number of nodes, elements and design variables of each model.

The initial values of each design variable used as first guess are presented in table 6. These values have been estimated for a blade with 2 webs and no ribs using the methodology presented in van Rijswijk et al.[5] To complete the dataset, the initial thickness of the core was set to 10 mm except for ribs where the initial value was set to 3 mm. The initial thickness of the composite layers in the ribs were also set to 1 mm each.

Table 5. Number of nodes, elements and design variables for each blade model studied in the sizing optimization step.

Models	Nodes	Elements	Design variables
2 webs, 0 rib	48 196	49 486	124
2 webs, 35 ribs	52 308	55 227	260
2 webs, 70 ribs	56 463	61 070	400
1 web, 0 rib	43 409	44 028	109
1 web, 35 ribs	47 769	49 769	245
1 web, 70 ribs	52 185	55 612	385

Table 6. First guess values (thicknesses in mm) of design variables for spar caps, webs, leading edge and trailing edge.

Sections [m]	Spar caps			Webs			Leading and trailing edges		
	UD	biaxial	Total	UD	biaxial	Total	UD	biaxial	Total
3.75–15	64.68	27.72	92.40	5.30	5.30	10.60	8.35	8.35	16.70
15–30	38.92	16.68	55.60	5.30	5.30	10.60	8.35	8.35	16.70
30–45	31.08	13.32	44.40	4.20	4.20	8.40	6.65	6.65	13.30
45–60	22.96	9.84	32.80	3.10	3.10	6.20	4.90	4.90	9.80
60–75	10.43	4.47	14.90	2.65	2.65	5.30	2.65	2.65	5.30

VI.B. Results

Table 7 shows the results of the sizing optimization of all blade models described in table 5. For both web configurations, the model with 35 ribs gives the lowest blade mass. When comparing blades with ribs against classic designs, it can be noticed that in general, the presence of ribs can result in a slight mass reduction. Furthermore, a blade with around 35 ribs seems to be the optimal topology.

For all models, all three optimization constraint types are actives. Analysis of failure index distribution over the blades showed that the failure index in the spar caps are in general much lower than the limit and also lower than in the leading edge, the trailing edge and the webs. It was also observed that the critical region for buckling is the upper trailing edge skin, where the buckling constraints is active for load case 3. For some blade models, buckling is also a critical constraints in the webs or in the ribs near the root for load case 4. A couple of elements in the leading edge, in the trailing edges and in the web reached the limit value of failure index. Based on these observations, it can be concluded that the thicknesses of spar caps are mainly driven by the rigidity constraints and that the thicknesses of webs, ribs, leading edge and trailing edge are driven by the buckling and/or the composite strength constraints.

Table 7. Results of sizing optimization: Optimized blade mass with associate active constraints

Model	Optimized mass [kg]	Active Constraints (load case)		
2 webs, 0 rib, PA-6/glass	30 272	defl. (3)	buck. (3)	fail. of 5 elem. (3)
2 webs, 35 ribs, PA-6/glass	29 861	defl. (3)	buck. (3, 4)	fail. of 3 elem. (1, 3, 4)
2 webs, 70 ribs, PA-6/glass	29 922	defl. (3)	buck. (3)	fail. of 2 elem. (3)
1 web, 0 rib, PA-6/glass	30 342	defl. (3)	buck. (3, 4)	fail. of 11 elem. (1, 3, 4)
1 web, 35 ribs, PA-6/glass	29 815	defl. (3)	buck. (3)	fail. of 2 elem. (1, 3)
1 web, 70 ribs, PA-6/glass	31 241	defl. (3, 4)	buck. (3)	fail. of 1 elem. (3)
2 webs, 0 rib, epoxy/glass	30 070	defl. (3)	buck. (3, 4)	fail. of 26 elem. (3, 4)
1 web, 0 rib, epoxy/glass	30 756	defl. (3)	buck. (3)	fail. of 41 elem. (1, 3, 4)

Table 8 shows the composite layer thicknesses, fraction of 0° UD fibers and core thicknesses for the section of the blade extending from 30 to 45 m. As the trends observed in this section are almost the same for the other sections, we will focus on this section to compare the different blade models.

VI.B.1. Spar caps

As it could have been predicted, spar caps are thicker than other parts of the blade because they support most of the load. In general, the thickness of spar caps are almost the same for all blade models except for the epoxy blades where the thicknesses are a little less because the rigidity of the epoxy/glass UD composite is slightly superior than the PA-6/glass UD composite.

The fraction of unidirectional fibers in the spar caps varies from 96 to 98 % to support the load that is predominantly in the axial direction of the blade. This value of UD fraction is a bit high when compared to what can be found in the litterature (70 %)[17,20] but the present optimization method does not consider torsional dynamic effects that could increase the need for $\pm 45°$ fibers.

VI.B.2. Leading edge and trailing edge skins

For models with 2 shear webs, the presence of ribs allows the skins to be thinner. When looking at table 8, it can be concluded that the mass saved because of the reduction of skin and web thickness is directly transferred to the ribs since the spar caps remain unchanged. If we compare the PA-6 composite blades with the epoxy-composite blades, we can also observe that the skin thickness of epoxy-composite blades is smaller or in the same range as skin thickness of PA-6 composite blades using ribs. This again can be explained by the fact that the epoxy/glass UD composite properties are slightly better than its PA-6 counterpart.

Lastly, the optimization processes yielded a fraction of UD fibers in the aerodynamic skins that ranges from 50 to 75 %. This is a little bit higher than what can be found in the literature. For exemple, Griffin et al.[20] uses about 40 % of UD in the skins in their baseline structural model.

VI.B.3. Webs

In general, the composite layers thickness of the webs (varying from 2.9 to 4.6 mm) does not seem to be affected by the number of ribs used in the blade structure. On the other hand, a clear increase in thickness between the two webs concept and the one web concept is noticeable. For both concepts, UD fraction goes from 47 to 71 % and has a tendency to increase with the number of ribs. Since the webs are submitted to important shear loads this large proportion of $\pm 45°$ seems logical and is in fact in line with what can be found in the litterature (50 %).[20]

VI.B.4. Ribs

Since the results showed that the 1/3 ratio between composite layers remained relatively stable during the optimization process (± 5 %), only the composite total thickness is shown in figure 10. The first thing noticeable on figure 10 is that rib thicknesses are, for most of the blade, thinner than the initial values. Because these parts are small compared to the skins and the spar caps, their influence on the objective function is not significant. Thus, the optimization problem converges before the rib thicknesses have reached their optimized values. This observation can be related to the fact that a reduction in rib thickness is noticeable from the tip to the blade mid-span. Ribs at mid-span are larger than ribs at tip so their influence on the objective function is more important, translating in a larger reduction in thickness. However, analysis of models optimized with 35 or 70 ribs shows that the buckling and composite strength constraints can not be respected if ribs are removed. This proves that the rib thicknesses from tip to blade mid-span could not converge to a value of 0.

At the root region, composite layer thicknesses are higher than the initial values indicating that ribs up to 5 mm thick are needed to avoid buckling of the ribs and the skins.

Finally, on a global level, one can notice localized rib thickening at the 15 m, 30 m and 45 m blade stations. As explained earlier, this corresponds to the areas where skin thickness changes from one section to the other (ply drop) forcing ribs to be slightly thicker to compensate local aerodynamic skin instability.

VI.B.5. Core thickness

The optimized core thickness is almost always lower than its initial value of 10 mm except in regions where buckling can be a concern. As for the ribs, the core being really light, it does not have an important effect on the objective function (mass). Therefore, the results obtained for regions not submitted to compressive loads are hard to interpret because core thicknesses may not have reached their optimized values before the

Table 8. Thickness of composite layers, UD fraction in composite layers and core thickness for the blade region extending from 30 m to 45 m.

		PA-6/Glass						Epoxy/Glass	
	Initial values	2 webs 0 rib	2 webs 35 ribs	2 webs 70 ribs	1 web 0 rib	1 web 35 ribs	1 web 70 ribs	2 webs 0 rib	1 web 0 rib
Up. surface leading edge skin	13.3 mm	4.1 mm	2.6 mm	2.3 mm	3.3 mm	3.2 mm	4.2 mm	2.4 mm	4.0 mm
	50 %	55.6 %	53.0 %	55.4 %	46.6 %	54.1 %	53.5 %	58.7 %	57.3 %
	10.0 mm	8.2 mm	7.1 mm	7.2 mm	9.6 mm	7.3 mm	8.1 mm	6.1 mm	7.9 mm
Upper surface spar cap	44.4 mm	88.0 mm	88.0 mm	87.9 mm	87.7 mm	85.6 mm	89.6 mm	83.5 mm	82.3 mm
	70 %	96.9 %	97.3 %	96.9 %	97.3 %	97.8 %	95.6 %	97.7 %	97.3 %
	10.0 mm	7.6 mm	6.6 mm	6.8 mm	10.3 mm	7.1 mm	8.1 mm	5.6 mm	7.4 mm
Up. surface trailing edge skin	13.3 mm	4.7 mm	2.4 mm	3.0 mm	3.6 mm	4.2 mm	5.3 mm	2.6 mm	3.1 mm
	50 %	40.6 %	22.7 %	16.0 %	37.3 %	15.5 %	26.8 %	49.6 %	63.6 %
	10.0 mm	20.4 mm	19.2 mm	15.4 mm	24.5 mm	14.5 mm	12.4 mm	23.9 mm	25.5 mm
Lower surface leading edge skin	13.3 mm	5.7 mm	4.5 mm	5.5 mm	3.8 mm	5.1 mm	10.2 mm	3.5 mm	4.4 mm
	50 %	63.7 %	62.9 %	61.7 %	61.1 %	65.6 %	71.8 %	68.1 %	59.6 %
	10.0 mm	8.2 mm	7.1 mm	7.3 mm	7.0 mm	7.4 mm	8.1 mm	6.1 mm	7.7 mm
Lower surface spar cap	44.4 mm	84.8 mm	84.5 mm	83.9 mm	80.3 mm	82.8 mm	80.4 mm	82.9 mm	80.7 mm
	70 %	96.8 %	97.3 %	98.0 %	98.1 %	97.6 %	95.5 %	97.0 %	97.3 %
	10.0 mm	7.5 mm	6.4 mm	6.7 mm	5.9 mm	6.9 mm	7.8 mm	5.0 mm	7.1 mm
Lower surface trailing edge skin	13.3 mm	2.4 mm	1.5 mm	0.8 mm	2.1 mm	1.6 mm	1.5 mm	2.5 mm	2.2 mm
	50 %	58.1 %	60.8 %	72.2 %	75.5 %	76.5 %	68.2 %	62.3 %	61.5 %
	10.0 mm	8.0 mm	8.3 mm	7.5 mm	12.6 mm	13.3 mm	8.9 mm	7.6 mm	10.6 mm
Center web	8.4 mm				4.2 mm	3.9 mm	3.5 mm		4.6 mm
	50 %				46.6 %	66.6 %	71.1 %		57.3 %
	10.0 mm				9.0 mm	8.9 mm	7.8 mm		8.5 mm
Aft web	8.4 mm	3.1 mm	2.9 mm	3.3 mm				3.4 mm	
	50 %	62.9 %	65.8 %	68.1 %				49.6 %	
	10.0 mm	8.7 mm	8.8 mm	7.8 mm				7.2 mm	
Forward web	8.4 mm	3.6 mm	2.6 mm	3.2 mm				2.0 mm	
	50 %	55.2 %	57.4 %	51.9 %				54.9 %	
	10.0 mm	8.4 mm	6.9 mm	7.2 mm				7.0 mm	

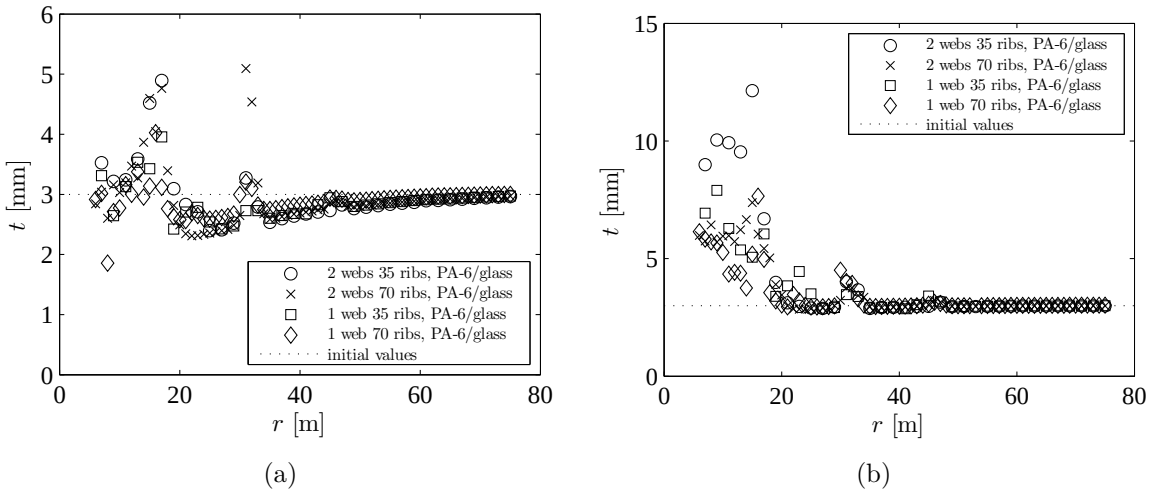

Figure 10. Rib thickness (t) along the blade span (r) for the different blade models. (a) Composite layers. (b) core.

optimization converged. However, core thicknesses in regions of the blade that are prone to buckle (upper and lower surface trailing edge skins) can be considered more optimum. As seen in table 8, core thickness in these regions varies from 12.4 to 24.5 mm and values increase as the number of webs and the number of ribs decrease. These results show the usefulness of core material to increase the buckling strength of parts submitted to compressive load. It also shows that the presence of ribs increases the buckling strength of the blade skins.

VI.B.6. Thickness variation along the blade span

Figure 11 shows the variation of composite layers thickness for different sections along the blade. In figure 11a, we can see that the maximum thickness of the upper spar cap (it is the same thing for the lower spar car) is situated at blade mid-span. Even if the bending moment is higher towards blade root, the reduction in thickness of the aerodynamic profiles towards blade tip causes the need for thicker laminates to reach values of section modulus that are sufficient to respect the maximum deflection constraints.

In other sections (lower surface leading edge (figure 11b), upper surface leading edge and upper surface trailing edge), the thickness of the composite layers tapers off towards blade tip in a more conventional way. For the other sections like the webs (figure 11c shows the aft webs) and the lower surface trailing edge, thicknesses reduce from the root to the middle of the blade and then increase towards the tip. This could again be explained by the fact that the reduction of thickness of the aerodynamic profiles towards the tip has to be counterbalanced by an increase of composite layer thicknesses.

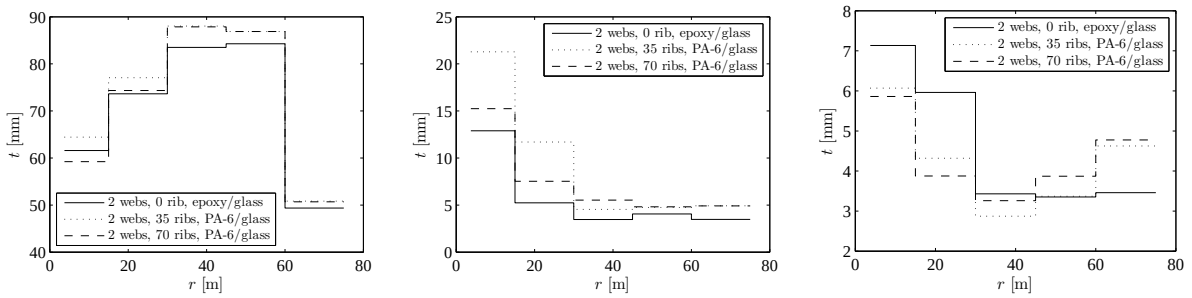

Figure 11. Composite layers thicknesses (t) along the blade span (r). (a) Upper surface spar cap. (b) Lower surface leading edge. (c) Aft web.

VII. Conclusion

It was argued in the introduction that to maximize the potential of TPC when used for wind turbine blade structures, it is essential to redesign the structure with respect to existing TPC material and manufacturing strong points. In that context, the authors believe that blade designs using ribs, multiple skin panels and stringers produced with fast non-isothermal melt processes could significantly help maximize the potential of TPC when used for wind turbine blade structures.

The optimization process presented in this study has shown that the use of ribs could be promising for construction of large thermoplastic wind turbine blades. The topology optimization step has shown that ribs appear to maximize the rigidity of the structure when a given amount of material is forced to be used. The sizing optimization step has shown that the use of ribs helps to reduce the thickness of aerodynamic shells and that a number of ribs around 35 (between 0 and 70) could be the optimum topology when the objective is to reduce the mass. The mass reduction being limited to about 1.5 %, it is hard to conclude that the rib concept has a major effect on blade mass reduction.

However, as just mentioned, a blade topology with ribs is well adapted for manufacturing processes using for thermoplastic composite. A structure with 2 webs is also well adapted for this process because the blade is clearly separated in three different structures: the spar, the leading edge and the trailing edge. Having three distinct sections gives this configuration an advantage over its one web counterpart. Working with a closed-cell main load carrying structural member helps in controlling load paths and minimizes the load transferred to the buckling prone trailing edge section. It also offers the possibility to easily manufacture

the box-spar in a different material than the leading edge and trailing edge section. As it was the case in the aeronautic industry, TPC composites could then first be used in wind turbine blade structure as secondary structure components (the box-spar still being made with thermoset composites). Gaining manufacturing experience with only these non-structural components could help manufacturers gain experience at minimal risk.

As future work, the next step of the design process would be to determine the number of plies of each type based on the layer thickness obtained in the sizing optimization and then, perform a stacking sequence optimization using the same objective and constraints as in the second step of the optimization process. This will lead to a more exact stress computation than with the SMCORE option (that supposes mostly in-plane loads).

Also, as it was shown by Jensen,[21] the failure of a wind turbine blade is highly dependent of non-linear effects due to the distortion of the aerodynamic shape of the section. These effects will have to be studied in the following steps of blade design. Nevertheless, since Jensen also showed that ribs can increase the strength of a blade when submitted to flapwise static loading by up to 30 %, the blade structural layout proposed in this paper is expected to limit these undesired cross-section distortions that are known to lead to premature blade failure.

References

[1]Veers, P. S., Ashwill, T. D., Sutherland, H. J., Laird, D. L., Lobitz, D. W., Griffin, D. A., Mandell, J. F., Musial, W. D., Jackson, K., Zuteck, M., Miravete, A., Tsai, S. W., and Richmond, J. L., "Trends in the Design, Manufacture and Evaluation of Wind Turbine Blades," *Wind Energy*, Vol. 6, 2003, pp. 245–259.

[2]Griffin, D. A., "Alternative Materials, Manufacturing Process and Structural Design for Large Wind Turbine Blades," *2002 ASME Wind Energy Symposium / 40th AIAA Aerospace Sciences Meeting and Exhibit*, Reno (Nevada, United States), 14–17 June 2002.

[3]"Global Market Scenario: Dynamics of the composites industry," 2009 release, JEC Composites.

[4]Joncas, S., de Ruiter, M. J., and van Keulen, F., "Preliminary Design of Large Wind Turbine Blades Using Layout Optimization Techniques," *10th AIAA/ISSMO Multidisciplinary Analysis and Optimization Conference*, Albany (New York, United States), 30 August – 1st September 2004.

[5]van Rijswijk, K., Joncas, S., Bersee, H., Bergsma, O., and Beukers, A., "Sustainable Vacuum-Infused Thermoplastic Composites for MW-Size Wind Turbine Blades - Preliminary Design and Manufacturing Issues," *Journal of Solar Energy Engineering*, Vol. 127, 2005, pp. 570–580.

[6]Joncas, S., Bergsma, O., and Beukers, A., "Power Regulation and Optimization of Offshore Wind Turbine through Trailing Edge Flap Control," *43rd AIAA Aerospace Sciences Meeting and Exhibit*, Reno (Nevada, United States), 10–13 January 2005.

[7]Timmer, W. and van Rooij, R., "Summary of the Delft University Wind Turbine Dedicated Airfoils," *Journal of Solar Energy Engineering*, Vol. 125, 2003, pp. 488–496.

[8]International Electrotechnical Commission, *Wind Turbine Generator Systems - Part 1 : Safety Requirements*, No. IEC 61400-1, International Electrotechnical Commission, Geneva (Switzerland), 2nd ed., 1999.

[9]Laino, D. J. and Hansen, A. C., "User's Guide to the Wind Turbine Aerodynamics Computer Software AeroDyn," 2002, `http://wind.nrel.gov/designcodes/simulators/aerodyn/AeroDyn.pdf`.

[10]Laino, D. J. and Hansen, A. C., "User's Guide to the Wind Turbine Dynamics Computer Program YawDyn," 2003, `http://wind.nrel.gov/designcodes/simulators/yawdyn/YawDyn.pdf`.

[11]Hansen, M. O., *Aerodynamics of Wind Turbines*, James & James, London (United Kingdom), 2nd ed., 2008.

[12]Bendsøe, M. and Sigmund, O., *Topology Optimization : Theory, Methods and Applications*, Springer-Verlag, Berlin, Heidelberg (Germany), 2003.

[13]Zhou, M., Pagaldipti, N., Thomas, H., and Shyy, Y., "An Integrated Apporach to Topology, Sizing and Shape Optimization," *Structural and Multidisciplinary Optimization*, Vol. 26, 2004, pp. 308–317.

[14]Thomas, H., Zhou, M., and Schramm, U., "Issues of Commercial Optimization Software Development," *Structural and Multidisciplinary Optimization*, Vol. 23, 2002, pp. 97–110.

[15]*Optistruct User Manual*, Altair Engineering, inc., Troy (Michigan, United States), 1999.

[16]de Ruiter, M. J., *Topology Optimization Using Topology Description Function Approach*, Ph.D. thesis, Delft University of Technology, Delft (The Netherlands), 2005.

[17]Berggreen, C., Branner, K., Jensen, J. F., and Schultz, J. P., "Application and Analysis of Sandwich Elements in the Primary Structure of Large Wind Turbine Blades," *Journal of Sandwich Structures and Materials*, Vol. 9, 2007, pp. 525–551.

[18]Joncas, S., van Rijswijk, K., Thibault-Liboiron, K., Bersee, H., and Beukers, A., "Mechanical Properties of Vacuum Infused Anionic Polyamide-6 (APA-6) Glass Fiber Composites: A Benchmark Study," *27th SAMPE Europe International Conference*, Paris (France), 27–29 March 2006.

[19]Nijssen, R., "OptiDAT Database Reference Document," Tech. Rep. 10224 (OB_TC_R018 rev. 005), 2006, `http://www.wmc.eu/optidat_files/Optidat%20reference%20document.pdf`, Database : `http://www.wmc.eu/optidat_files/Optidat__public.zip`.

[20]Griffin, D. A. and Zuteck, M. D., "Scaling of Composite Wind Turbine Blades for Rotor of 80 to 120 Meter Diameter," *Journal of Solar Energy Engineering*, Vol. 123, 2001, pp. 310–318.

[21] Jensen, F. M., *Ultimate Strength of a Large Wind Turbine Blade*, Ph.D. thesis, Risø National Laboratory for Sustainable Energy, Technical University of Denmark, Roskilde (Denmark), 2008.